



Synthesis and characterization of DNL-6, a new silicoaluminophosphate molecular sieve with the RHO framework

Xiong Su^{a,b,c}, Peng Tian^{a,b}, Jinzhe Li^{a,b}, Ying Zhang^{a,b}, Shuanghe Meng^{a,b}, Yanli He^{a,b}, Dong Fan^{a,b,c}, Zhongmin Liu^{a,b,*}

^aNational Engineering Laboratory for Methanol to Olefins, Dalian Institute of Chemical Physics, Chinese Academy of Sciences, P.O. Box 110, 116023 Dalian, PR China

^bDalian National Laboratory for Clean Energy, Dalian Institute of Chemical Physics, Chinese Academy of Sciences, Dalian, PR China

^cGraduate University of Chinese Academy of Sciences, Beijing 100049, PR China

ARTICLE INFO

Article history:

Received 3 September 2010

Received in revised form 25 March 2011

Accepted 4 April 2011

Available online 13 April 2011

Keywords:

SAPO

RHO

Synthesis

DNL-6

Crystallization mechanism

ABSTRACT

A new silicoaluminophosphate molecular sieve with the RHO framework (designated as DNL-6, Dalian National Laboratory Number 6) has been hydrothermally synthesized for the first time with diethylamine (DEA) template in the presence of cetyltrimethylammonium bromide (CTAB). Influence factors, such as CTAB amount and silica content in the starting gel, crystallization time and temperature, were investigated. It was observed that DEA together with CTAB were necessary for the formation of pure RHO phase, which appeared in a narrow range of the starting gel compositions and synthesis conditions. Only DEA and water molecules were found in the as-synthesized DNL-6 without any existence of CTAB. All Si atoms incorporated into the framework with Si(4Al) environment at a high amount close to the theoretical maximum value. DNL-6 molecular sieve possessed high micropore surface area (777 m²/g) and large micropore volume (0.36 cm³/g) with good thermal and hydrothermal stability. Crystallization course was studied by monitoring solid products at different crystallization times with XRD, SEM, XRF, NMR and CHN elemental analysis. It is proposed that DNL-6 crystals were more likely formed directly from the crystallization of liquid phase rather than from the transformation of amorphous materials, and Si atoms directly incorporated into the DNL-6 framework from the very beginning of the crystallization via a SM2 mechanism.

© 2011 Elsevier Inc. All rights reserved.

1. Introduction

Molecular sieves have been widely used in many industrial fields as sorbents, catalysts and ion exchangers [1,2]. Increasing numbers of new framework types with compositional variability have been synthesized in recently years due to the impressive synthetic efforts [3], providing more chance for understanding of crystallization mechanisms and for practical application. However, rational design of novel materials with targeted properties (structure, composition, morphology, etc.) still remains a challenge, although some evident progress has been made by several research teams [4–7].

Union Carbide firstly reported aluminophosphate (AIPO) and silicoaluminophosphate (SAPO) molecular sieves in 1980s, which are formed by the self-assembling of tetrahedrally connected TO₄ (T = Si, Al, P, etc.) building units with the assistance of organic directing agents [8–11]. AIPO and SAPO molecular sieves contain

many different framework types, in which some are analogous to certain known zeolites, but a large numbers have unique structures [12]. Since their discovery, some important industrial applications have been developed. For example, SAPO-11 was used as catalyst for hydroisomerization of long-chain paraffins [13] and SAPO-34 as catalyst for methanol to olefin (MTO) reaction [14].

Aluminosilicate zeolite RHO, firstly reported by Robson, is often synthesized in the presence of sodium and cesium cations [15]. The body-centered cubic symmetry structure of RHO is composed of α -cages linking through double 8-rings (D8R) with pore size of 3.6 × 3.6 Å. This structure would undergo a framework distortion with change of unit cell symmetry or even collapse upon extra framework cation exchange or dehydration [16–18]. Extensive pioneer works have shown that zeolite RHO owns excellent performance for selective synthesis of dimethylamine from methanol and ammonia [19,20]. However, the use of expensive cesium cations in the synthesis of RHO zeolite is a limitation on its application. Other RHO analogs, containing berylllophosphate [21], beryllloarsenate [22], aluminogermanate [23], ECR-10 [20], LZ-214 [24], have also been synthesized with inorganic cations as structure directing agents. Me-AIPOs (Me = Co, Mg, Mn) RHO analogs were reported using organic amine as structure directing

* Corresponding author at: Dalian National Laboratory for Clean Energy, Dalian Institute of Chemical Physics, Chinese Academy of Sciences, Dalian, PR China. Tel.: +86 411 84685510; fax: +86 411 84691570.

E-mail address: liuzm@dicp.ac.cn (Z. Liu).

agent, but their framework structures were unstable upon the removal of organic templates [25].

In this paper, we report the synthesis of DNL-6, a new silicoaluminophosphate molecular sieve with RHO-type framework, by using DEA as the template in the presence of CTAB surfactant. Si incorporation and crystallization mechanism were discussed based on the investigation of the entire crystallization process. During the present synthesis research, our group found that DNL-6 could also be prepared through a phase-transition method from the SAPO-5 precursor [26].

2. Experimental

2.1. Synthesis

Typical hydrothermal synthesis procedure was as follows. Orthophosphoric acid (85 wt.%) and tetraethyl orthosilicate were mixed with a solution of aluminium isopropoxide and deionized water, and then an aqueous solution of cetyltrimethylammonium bromide (CTAB) was added with final addition of DEA template. Stirring was kept during all the above mixing procedure. The final gel mixture was transferred into a stainless-steel autoclave and heated up to 200 °C under rotation. Crystallization time was recorded once the temperature reached 200 °C. After certain time at the temperature for crystallization, the autoclave was cooled down and the solid product was recovered by filtration, washed three times with deionized water and further three times by ethanol, and dried at 110 °C overnight. Calcination was carried out at 600 °C for 4 h to remove organic species. The detailed gel compositions for the hydrothermal synthesis of DNL-6 are given in Table 1.

To investigate the crystallization mechanism, some experiments were performed with different crystallization times in separate batches from the same gel composition of 1.0DEA:1.0Al:0.8P:0.2Si:0.1CTAB:50H₂O.

2.2. Characterization

Powder X-ray diffraction (XRD) patterns were recorded on a PANalytical X'Pert PRO X-ray diffractometer with Cu K α radiation ($\lambda = 0.15418$ nm). Scanning electron microscopy (SEM) images were taken on a KYKY-AMRAY-1000B electron microscope at 25 kV. Chemical composition was determined with an X-ray fluorescence (XRF) spectrometer (Philips Magix-601). CHN elemental analysis was measured using VARIO EL III elemental analyzer (Germany Elementar Company). N₂ adsorption measurement was carried out on a Micromeritics 2010 analyzer at 77.35 K after the sample was degassed at 350 °C under vacuum. MAS NMR measurements were conducted on a Varian Infinity plus 400 WB spectrometer, where resonance frequencies were 79.41, 104.17, 161.83 and 100.5 MHz for ²⁹Si, ²⁷Al, ³¹P and ¹³C, respectively. Spinning rates of the samples at the magic angle were 4, 10, 6 and 8 kHz for ²⁹Si, ²⁷Al, ³¹P and ¹³C, respectively. Reference materials for the chemical

shift (in ppm) determination were 2,2-dimethyl-2-silapentane-5-sulfonate sodium salt (DSS) for ²⁹Si and ¹³C, 1.0 M Al(H₂O)₆³⁺ for ²⁷Al and 85% H₃PO₄ for ³¹P. Thermal analysis was carried out on a TA Q600 analyzer at a heating rate of 10 °C/min under an airflow rate of 100 ml/min.

Relative crystallinity of the samples was calculated by the formula: $I_{rel.(\%)} = (I_1 + I_2 + I_3)_{sample} \times 100 / (I_1 + I_2 + I_3)_{standard}$, where I_n ($n = 1, 2, 3$) represents the intensities of the three strongest diffraction peaks on the XRD pattern. The sample crystallized at 200 °C for 24 h was chosen as a standard one.

3. Results and discussion

3.1. Synthesis

The detailed synthetic conditions of samples are shown in Table 1. In the case of no CTAB addition to the gel, it could be seen from Table 1 (C1) that only small amount of RHO was observed, coexisting with the main product of CHA phase. This is partly consistent with our previous research, in which CHA was the only product [27]. Addition of small amount of CTAB (C2, 0.05 mol) to the gel led to a product mainly in RHO phase. Increase of CTAB (C3, C4) gave a pure RHO phase. However, further increase of CTAB (C5, 0.2 mol) would cause the formation of an amorphous product. Pure RHO phase appeared only in a narrow CTAB range (0.1–0.15 mol). The above results indicate that DEA together with CTAB were necessary for the formation of RHO phase, which was also sensitive to the amount of CTAB in the starting gel.

Silica content effect was investigated by keeping CTAB at an optimized amount for the formation of pure RHO phase. It is evident that from S1, C3, S2 and S3 samples in Table 1, the change of silica contents in the gel caused different solid products, without pure RHO phase except for C3. Similar phenomena were observed when changing crystallization time and temperature. Longer crystallization time (T2, 48 h) led to a mixture of RHO and CHA. Decreasing crystallization temperature to 180 °C, RHO formed together with amorphous solids.

For most investigations in the syntheses, an interesting phenomenon is the coexistence of RHO and CHA phases. A reasonable explanation is that RHO and CHA have the same loop configuration of T-atoms in their frameworks, and similar coordination sequences from N1 to N4 [3].

3.2. Physicochemical characterization of DNL-6

The sample C3 in Table 1 was used for various physicochemical characterizations.

3.2.1. XRD, XRF and SEM

The XRD patterns of the samples are shown in Fig. 1. Peak positions of as-synthesized sample C3 were almost identical to those of the aluminosilicate RHO zeolite except the difference in the

Table 1
Gel compositions and resultant products of hydrothermal synthesis.

Sample	Al	P	Si	DEA	CTAB	H ₂ O	Time (h)	Product phase
C1	1	0.8	0.2	1	0	50	24	CHA + small RHO
C2	1	0.8	0.2	1	0.05	50	24	RHO + small CHA
C3	1	0.8	0.2	1	0.1	50	24	RHO
C4	1	0.8	0.2	1	0.15	50	24	RHO
C5	1	0.8	0.2	1	0.2	50	24	Amorphous
S1	1	0.8	0.0	1	0.1	50	24	Amorphous + minor RHO + minor CHA
S2	1	0.8	0.3	1	0.1	50	24	RHO + minor CHA
S3	1	0.8	0.4	1	0.1	50	24	CHA
T1 ^a	1	0.8	0.2	1	0.1	50	24	RHO + small amorphous
T2	1	0.8	0.2	1	0.1	50	48	RHO + CHA

^a Crystallization temperature was 180 °C.

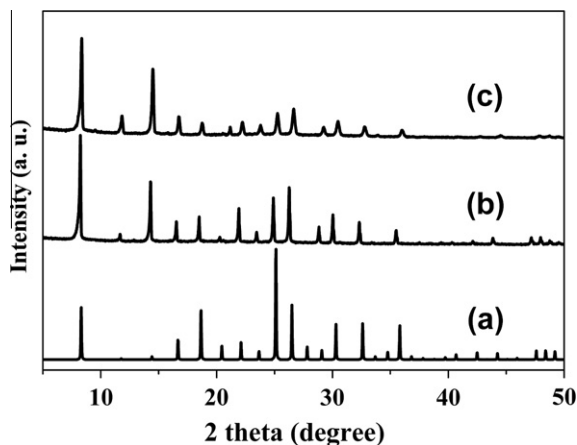


Fig. 1. XRD patterns of (a) RHO zeolite from database (b) as-synthesized DNL-6 and (c) DNL-6-950.

relative peak intensities, which could be indexed to the topology of RHO framework.

The bulk composition of sample C3 was determined by XRF and calculated to give a molar ratio of $\text{Si}_{0.135}\text{Al}_{0.496}\text{P}_{0.369}\text{O}_2$, ensuring that the sample is a SAPO molecular sieve. CHN elemental analysis showed that the C/N atomic ratio of C3 was 4/1, equal to the ratio of DEA, suggesting that no CTAB but only DEA was occluded in the as-synthesized sample. This was also confirmed by ^{13}C MAS NMR measurement (see Fig. 3), where only signals from DEA centered at 12 and 43 ppm were observed. These results are reasonable because CTAB was normally used in the synthesis of mesoporous materials to create mesopores, and CTAB could not direct crystallization of microporous crystals. However, the exact effect of CTAB in the synthesis of DNL-6 is still interesting and worthy of further research.

SEM image (Fig. 2a) of as-synthesized DNL-6 shows that only truncated rhombic dodecahedron crystals existed, suggesting high purity of the sample. Moreover, DNL-6 with perfect rhombic dodecahedral morphology could be occasionally obtained (Fig. 2b), similar to that of RHO zeolite reported by Newsam et al. [20].

3.2.2. MAS NMR spectra

Chemical environments of the framework atoms in the as-synthesized DNL-6 were measured by solid-state MAS NMR. The results are shown in Fig. 4 (24 h).

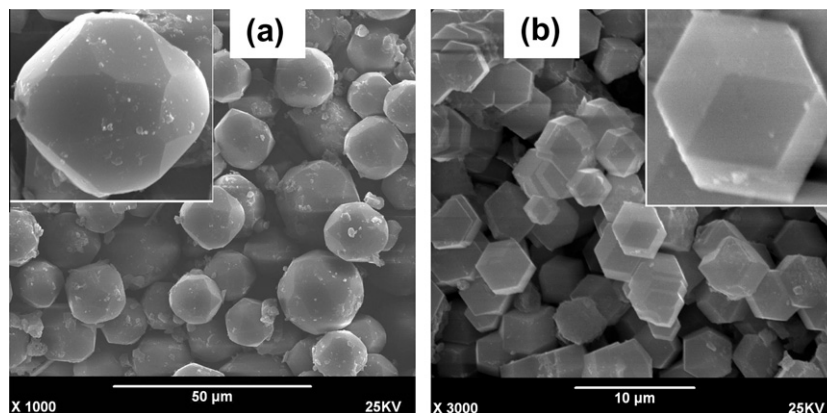


Fig. 2. SEM images of the as-synthesized DNL-6 (sample C3 as defined in Table 1). Two morphologies could be obtained under the synthesis condition – (a) truncated rhombic polyhedron and (b) rhombic dodecahedron.

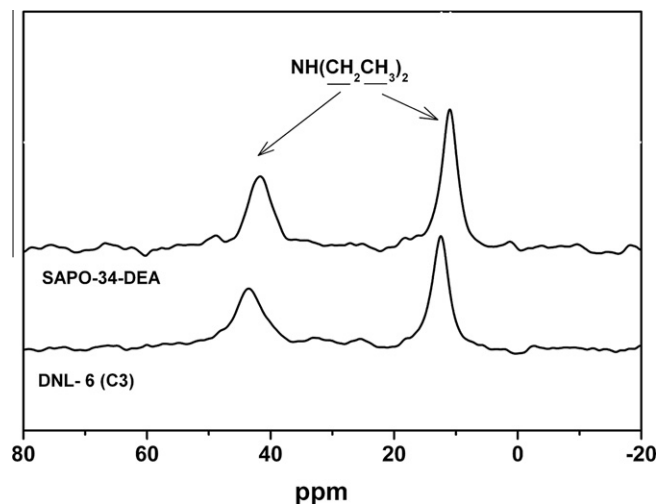


Fig. 3. ^{13}C MAS NMR spectra of the as-synthesized samples. SAPO-34-DEA means that SAPO-34 was synthesized with only DEA template.

^{31}P MAS NMR spectrum gave a peak at -28.7 ppm corresponding to $\text{P}(\text{OAl})_4$ resonance [28]. In the ^{29}Si MAS NMR spectrum, only one resonance peak was observed at -92.3 ppm that could be assigned to $\text{Si}(4\text{Al})$ environment [29]. Considering the high Si content in the sample ($\text{Si}_{0.135}\text{Al}_{0.496}\text{P}_{0.369}\text{O}_2$), it is suggested that the framework of DNL-6 can accommodate high amount of single Si environment, close to the theoretical maximum [30]. Two resonance peaks existed in the ^{27}Al MAS NMR spectrum of as-synthesized DNL-6. One was at 8.2 ppm corresponding to tetrahedrally coordinated Al environment; another peak centered at 9.1 ppm should be ascribed to penta-coordinated Al environment, arising from additional interaction of water or template molecule to the framework alumina [31]. However, upon calcination the spectrum became simple and contained only one peak at chemical shift of 38.9 ppm, assigned to tetrahedrally coordinated Al atoms. It is noted that there was a difference in the chemical shifts of tetrahedrally coordinated Al atoms between the as-synthesized sample and the calcined sample, suggesting the interaction of DEA and H_2O molecules with AlO_4^- species.

3.2.3. Thermal analysis

Fig. 5 presents TG-DTG and DSC analysis results of the as-synthesized DNL-6 sample. The first weight loss of 4.85% before 200°C with an endothermic effect could be attributed to desorp-

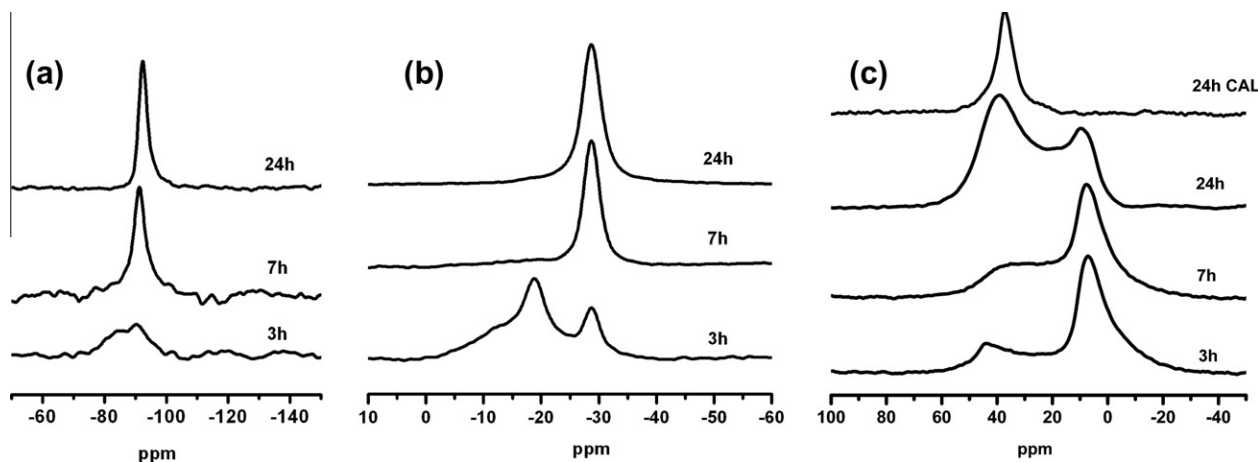


Fig. 4. ^{29}Si (a), ^{31}P (b) and ^{27}Al MAS NMR (c) spectra of as-synthesized samples with different crystallization times. CAL represented the calcined sample. (gel molar composition 1.0DEA:1.0Al:0.8P:0.2Si:0.1CTAB:50H₂O, $T = 473$ K).

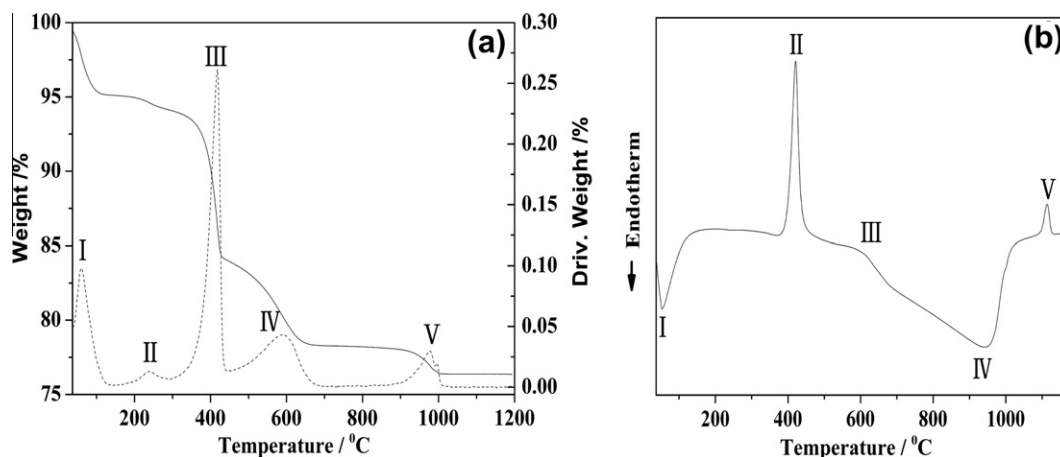


Fig. 5. (a) TG-DTG and (b) DSC curves of the as-synthesized DNL-6 sample.

tion of physically adsorbed water. In the higher temperature range from 200 to 650 °C, a total weight loss of 16.81% (three stages II, III and IV) appeared with a sharp exothermic peak and a slight exothermic change in the DSC pattern due to the combustion of organic molecules. Because there was no CTAB occluded in the as-synthesized sample, the weight loss in these three stages should be related to the removal of DEA template. The final weight loss of ~1.5% (stage V) appeared at 970 °C with an endothermic peak on DSC curve, which is interesting and not yet reported for other SAPO materials. In order to understand the origin of this weight loss, a powder sample was calcined at 950 °C for 1 h (designated as DNL-6-950) for further characterization. XRF analysis revealed that the inorganic elemental composition of DNL-6-950 remained the same as that of as-synthesized sample. XRD result showed that DNL-6-950 kept the RHO topology with a little decrease of diffraction intensity (see Fig. 1). Thus, the weight loss at stage V was assigned to the condensation of hydroxyl from the framework. Fur-

ther increasing the temperature, an exothermic peak at 1100 °C appeared on the DSC curve without any appreciable weight loss on the TG curve, corresponding to the collapse of DNL-6 framework.

Table 2 summarized the detailed weight losses. Based on the topological structure of DNL-6 molecular sieve, i.e., each unit cell (two cages) containing 48 T sites, the number of removable molecules per cage were calculated to be 4.28 DEA and 5.00 H₂O. The template number in each cage of DNL-6 was obviously higher than that of SAPO-34-DEA (1.74) [27], in accordance with the larger cage in the RHO framework.

3.2.4. Hydrothermal stability

High temperature steam treatment (800 °C, 8 h, 100% steam) was carried out in order to investigate the hydrothermal stability of DNL-6. N₂ adsorption-desorption isotherms and textural properties of the samples before and after the treatment are shown in Fig. 6 and Table 3, respectively.

Table 2
Thermal analysis results of DNL-6.

Sample	Weight loss (%)					Moles of water per cage	Moles of DEA per cage
	I	II	III	IV	V		
DNL-6	4.85	0.87	10.19	5.75	1.82	5.00	4.28

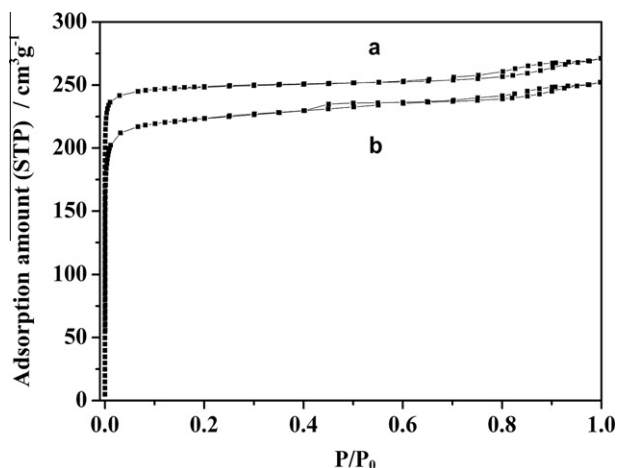


Fig. 6. N_2 adsorption–desorption isotherms of DNL-6 after (a) calcination at 600 °C for 4 h and (b) steam treatment at 800 °C for 8 h.

Table 3
Textural properties of DNL-6 before and after hydrothermal treatment.

Sample	Relative crystallinity (%)	Surface area (m^2/g)			Pore volume (cm^3/g)	
		S_{micro}	S_{ext}^a	S_{total}^b	V_{micro}^c	V_{total}
DNL-6	100	777	51	828	0.36	0.42
DNL-6-HT	80	658	89	747	0.31	0.39

^a *t*-Plot external surface area.

^b BET surface area.

^c *t*-Plot micropore volume.

Normally calcined sample gives a Type I adsorption–desorption isotherm with an extra weak uptake slope in the range of 0.7–0.9 (P/P_0). Micropore surface area and micropore volume were calculated to be 777 m^2/g and 0.36 cm^3/g . After steam treatment, 80% of the relative crystallinity remained, and both the total surface area and pore volume decreased by *ca.* 15%, respectively. This implies that DNL-6 is a highly hydrothermal stable molecular sieve.

3.3. Crystallization course

Solid products with different crystallization times were characterized using XRD, SEM, NMR, XRF, CHN elemental analysis, etc. These results are shown in Figs. 4, 7, 8 and Table 4.

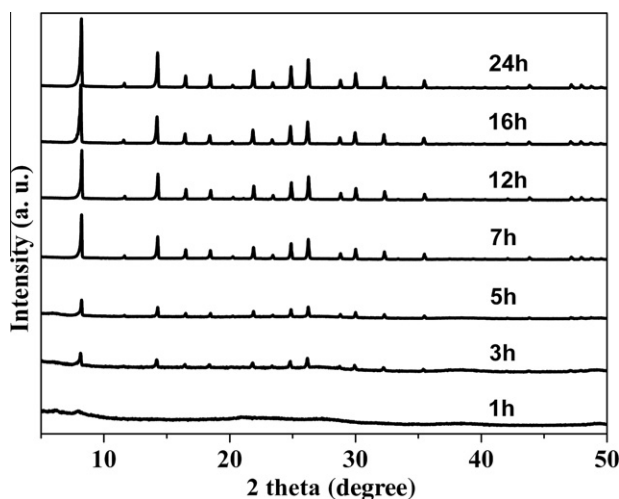


Fig. 7. XRD patterns of DNL-6 synthesized with different crystallization times.

It could be seen from Fig. 7 that at the initial 1 h, the product was mostly in amorphous phase with a very weak diffraction peak at $2\theta = 8.2^\circ$, corresponding to the RHO phase. The diffraction peaks of DNL-6 became more evident at 3 and 5 h. The sharp increase of the relative crystallinity appeared from 5 h (16%) to 7 h (72%). Afterwards, the intensities of diffraction peaks increased gradually with time and the relative crystallinity reached 100% at 24 h.

From SEM images of the samples (Fig. 8), amorphous material without uniform shapes was observed at 1 h. Although XRD results indicated that there was a weak DNL-6 diffraction peak, however, it is difficult to find a crystal in the product at this time. After 3 h, small amount of solids with sphere-like morphology appeared together with amorphous solids. Considering the corresponding XRD result, the sphere particles should be DNL-6 crystals. When at 7 h, more crystals could be observed with amorphous materials accumulating onto the sphere surface. Further prolonging the crystallization time, the amount of amorphous materials decreased gradually with the faces and edges of crystals becoming much clearer, which was in consistency with the high crystallinity of the sample.

The change of MAS NMR results with crystallization time are shown in Fig. 4. In the early stage of crystallization (3 h), the wide peak higher than -90 ppm in the spectrum of ^{29}Si MAS NMR should be assigned to Si species in the amorphous Si–Al patch [32]; the broad peaks centered at -18 ppm in the ^{31}P MAS NMR spectrum could be assigned to P species with low degree of condensation [33]; the strong peak at 7 ppm in the ^{27}Al MAS NMR spectrum indicated the existence of amorphous alumina [34]. Although the solid products in this early stage normally contained amorphous phase, there were still evident resonances of Si(4Al), P(4Al), and tetrahedrally coordinated Al environments, suggesting that Si directly incorporated into the framework to form the crystals. This is in agreement with the SM2 substitution mechanism for the formation of SAPO framework [29].

Table 4 listed various measurement and analysis data of the solid products during crystallization. It could be seen that chemical compositions of the samples varied during the whole crystallization course. Yields of solid products changed in a relatively narrow range of 48–66%, implying that there existed a lot of amorphous phase in the solid product when relative crystallinity was low, which is in accordance with SEM observations. For the framework construction of SAPOs, due to the absence of Si–O–P linkages, the number of Al atoms should be equal to the number of Si plus P atoms when Si atoms in Si(4Al) state. Al/(Si + P) values of the samples approached to one while crystallization time was longer than 16 h, indicating that the crystal product was in high purity, and the Si atoms should be in Si(4Al) environment. These were consistent with MAS-NMR results. The values of Al/(Si + P) greater than one in the early crystallization stage implies that the amorphous phase was rich in Al species. Furthermore, CTAB/DEA ratio deduced from CHN elemental analysis in Table 4 indicates that CTAB could be only founded in amorphous phase. Considering the solid products being washed by water and ethanol for several times, there should exist a strong interaction between CTAB and amorphous materials.

3.4. Crystallization mechanism

It is interesting to know how DNL-6 crystals were formed during the crystallization course. There are generally two typical mechanisms for the transformation of starting gel to crystals: (1) crystals directly transformed from amorphous phase (solid-phase transport mechanism) and (2) crystals formed from liquid phase (solution-mediated transport mechanism). In the case of DNL-6 synthesis, if the crystals were directly transformed from amorphous phase, it is expected that there should be a strong combination of crystals and amorphous phase, and a corresponding

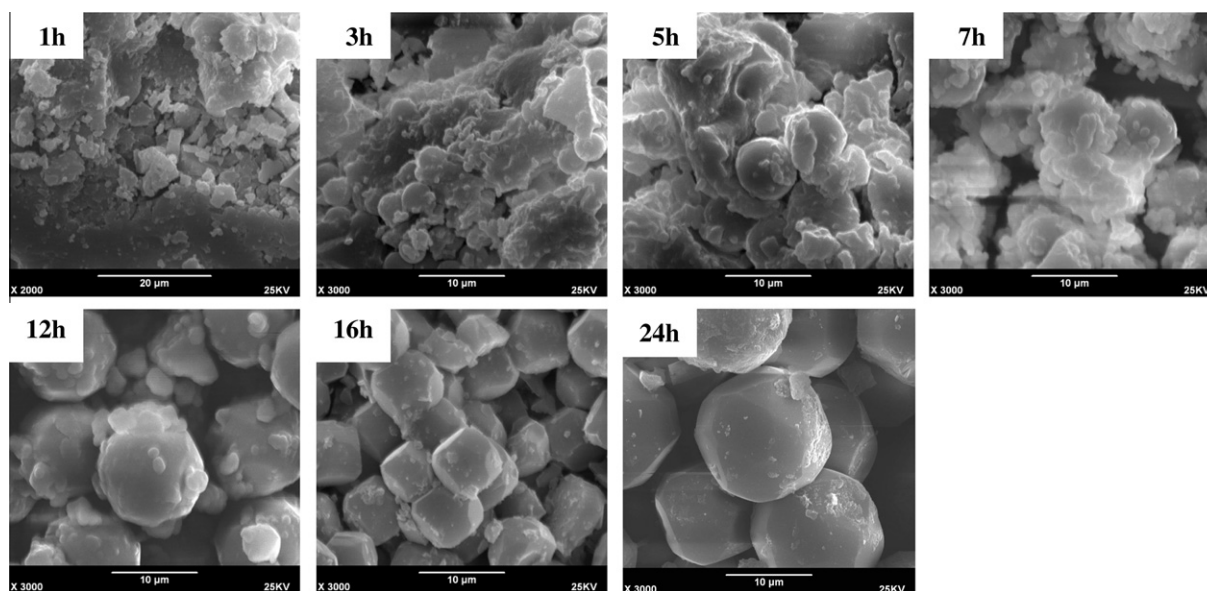


Fig. 8. SEM images of samples with different crystallization times.

Table 4
Compositions and yields of samples with different crystallization times.

Time (h)	Molar composition	Yield (%)	Relative crystallinity (%)	Al/(Si + P)	C/N molar ratio ^a	CTAB/DEA molar ratio ^b
1	Si _{0.134} Al _{0.588} P _{0.279} O ₂	49	0	1.42	–	
3	Si _{0.134} Al _{0.610} P _{0.256} O ₂	48	7	1.56	11.2	1.0
5	Si _{0.135} Al _{0.598} P _{0.267} O ₂	62	16	1.49	–	
7	Si _{0.126} Al _{0.582} P _{0.292} O ₂	66	72	1.39	7.4	0.3
12	Si _{0.123} Al _{0.572} P _{0.305} O ₂	66	85	1.34	–	
16	Si _{0.130} Al _{0.495} P _{0.375} O ₂	59	89	0.98	4.1	0
24	Si _{0.135} Al _{0.496} P _{0.369} O ₂	65	100	0.98	4.0	0

^a By CHN elemental analysis.

^b Calculated based on the value of C/N molar ratio.

transition region could be possibly observed. Therefore, the sample with 7 h crystallization time was selected for further SEM investigation (see Fig. 9). It is clear that after further washing the sample by ethanol and trying mechanical crush, uniform crystals with clear faces and edges was observed. Moreover, elemental compositions of products changed always during the crystallization course. Based on the above discussions, we propose that the synthesis of DNL-6 crystals possibly passed through a liquid-phase transformation mechanism, i.e., the crystals directly formed from the crystallization of liquid phase, to which the amorphous phase providing

nutrition elements through dissolution. This could explain why there was no CTAB in DNL-6. Additionally, Si species from the liquid phase directly incorporated into the DNL-6 framework since the very beginning of the crystallization with a SM2 mechanism.

4. Conclusions

A new silicoaluminophosphate molecular sieve DNL-6 has been hydrothermally synthesized, in which DEA together with CTAB are

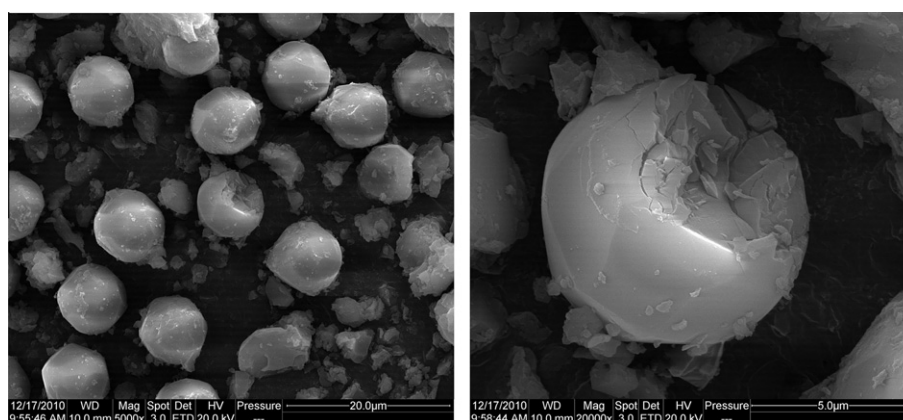


Fig. 9. SEM images of sample with crystallization time of 7 h after further washing by ethanol and mechanical crush.

necessary for the structure formation. Pure DNL-6 appeared in a narrow composition range of the starting gel and also in a narrow range of synthesis conditions. DEA and water molecules, but no CTAB, were found in the as-synthesized DNL-6. All Si atoms incorporated into the framework with Si(4Al) environment at a high amount close to the theoretical maximum value. DNL-6 possessed high micropore surface area (777 m²/g) and large micropore volume (0.36 cm³/g) with good thermal and hydrothermal stability. It is proposed that DNL-6 crystals were more likely formed directly from the crystallization of liquid phase, and Si atoms directly incorporated into the framework from the initial crystallization with a SM2 mechanism.

Acknowledgement

We thank Prof. Qinghua Xia for his helpful discussions and language revision on this manuscript.

References

- [1] A. Corma, *Chem. Rev.* 95 (1995) 559.
- [2] M.E. Davis, *Nature* 417 (2002) 813.
- [3] Ch. Baerlocher, L.B. McCusker, Database of Zeolite Structures. Available from: <<http://www.iza-structure.org/databases/>>.
- [4] M. Castro, R. Garcia, S.J. Warrender, A.M.Z. Slawin, P.A. Wright, P.A. Cox, A. Fecant, C. Mellot-Draznieks, N. Bats, *Chem. Commun.* (2007) 3470.
- [5] E.J. Fayad, N. Bats, C.E.A. Kirschhock, B. Rebours, A.–A. Quoineaud, J.A. Martens, *Angew. Chem. Int. Ed.* 49 (2010) 4585.
- [6] Z.X. Han, A.L. Picone, A.M.Z. Slawin, V.R. Seymour, S.E. Ashbrook, W.Z. Zhou, S.P. Thompson, J.E. Parker, P.A. Wright, *Chem. Mater.* 22 (2010) 338.
- [7] M. Choi, K. Na, J. Kim, Y. Sakamoto, O. Terasaki, R. Ryoo, *Nature* 461 (2009) 246.
- [8] S.T. Wilson, B.M. Lok, C.A. Messina, T.R. Cannan, E.M. Flanigen, *J. Am. Chem. Soc.* 104 (1982) 1146.
- [9] S.T. Wilson, B.M. Lok, E.M. Flanigen, US Patent 4310440, 1982.
- [10] B.M. Lok, C.A. Messina, R.L. Patton, R.T. Gajek, T.R. Cannan, E.M. Flanigen, *J. Am. Chem. Soc.* 106 (1984) 6092.
- [11] B.M. Lok, C.A. Messina, R.L. Patton, R.T. Gajek, T.R. Cannan, E.M. Flanigen, US Patent 4440871, 1984.
- [12] J.H. Yu, R.R. Xu, *Acc. Chem. Res.* 36 (2003) 481.
- [13] S.J. Miller, A.J. Dahlberg, K.R. Krishna, R.R. Kryg, US Patent 2001006155-A1, 2001.
- [14] Z. Liu, C. Sun, G. Wang, Q. Wang, G. Cai, *Fuel Process. Tech.* 62 (2000) 161.
- [15] H.E. Robson, D.P. Shoemaker, R.A. Ogilvie, P.C. Manor, *Adv. Chem. Ser.* 121 (1973) 106.
- [16] L.B. McCusker, *Zeolites* 4 (1984) 51.
- [17] A. Bieniok, K.D. Hammonds, *Micropor. Mesopor. Mater.* 25 (1998) 193.
- [18] D.R. Corbin, L. Abrams, G.A. Jones, M.M. Eddy, W.T.A. Harrison, G.D. Stucky, D.E. Cox, *J. Am. Chem. Soc.* 112 (1990) 4821.
- [19] R.D. Shannon, M.J. Keane, L. Abrams, R.H. Staley, T.E. Gier, D.R. Corbin, G.C. Sonnichsen, *J. Catal.* 133 (1988) 367.
- [20] J.M. Newsam, D.E.W. Vaughan, K.G. Strohmaier, *J. Phys. Chem.* 99 (1995) 9924.
- [21] G. Harvey, W.M. Meier, *Stud. Surf. Sci. Catal.* 49 (1989) 411.
- [22] T.E. Gier, G.D. Stucky, *Nature* 349 (1991) 508.
- [23] G.M. Johnson, A. Tripathi, J.B. Parise, *Micropor. Mesopor. Mater.* 28 (1999) 139.
- [24] D.W. Breck, G.W. Skeels, US Patent 4503023, 1985.
- [25] P.Y. Feng, X.H. Bu, G.D. Stucky, *Micropor. Mesopor. Mater.* 23 (1998) 315.
- [26] P. Tian, X. Su, Y.X. Wang, Q.H. Xia, Y. Zhang, D. Fan, S.H. Meng, Z.M. Liu, *Chem. Mater.* 23 (2011) 1406.
- [27] G.Y. Liu, P. Tian, J.Z. Li, D.Z. Zhang, F. Zhou, Z.M. Liu, *Micropor. Mesopor. Mater.* 111 (2008) 143.
- [28] A. Buchholz, W. Wang, A. Arnold, M. Xu, M. Hunger, *Micropor. Mesopor. Mater.* 57 (2003) 157.
- [29] R. Vomscheid, M. Briend, M.J. Peltre, P.P. Man, D. Barthomeuf, *J. Phys. Chem.* 98 (1994) 9614.
- [30] L.S. Saldarriaga, C. Saldarriaga, M.E. Davis, *J. Am. Chem. Soc.* 109 (1987) 2686.
- [31] C.S. Blackwell, R.L. Patton, *J. Phys. Chem.* 92 (1988) 3965.
- [32] M. Derewinski, M.J. Peltre, M. Briend, D. Barthomeuf, P.P. Man, *J. Chem. Soc., Faraday Trans.* 89 (1993) 1823.
- [33] J. Xu, D. Zhou, X.W. Song, L. Chen, J.H. Yu, C.H. Ye, F. Deng, *Micropor. Mesopor. Mater.* 115 (2008) 576.
- [34] J. Tan, Z.M. Liu, X.H. Bao, X.C. Liu, X.W. Liu, C.Q. He, R.S. Zhai, *Micropor. Mesopor. Mater.* 53 (2002) 97.